Haas, M., Agnon, A., Bindi, D., Parolai, S., Pittore, M. (2016): Data-Driven Seismic-Hazard Models Prepared for a Seismic Risk Assessment in the Dead Sea Region. - *Bulletin of the Seismological Society of America*, *106*, 6, pp. 2584—2598.

DOI: http://doi.org/10.1785/0120150361

THE SEISMOLOGICAL SOCIETY OF AMERICA
400 Evelyn Ave., Suite 201
Albany, CA 94706-1375
(510) 525-5474; FAX (510) 525-7204
www.seismosoc.org

Bulletin of the Seismological Society of America, Vol. 106, No. 6, pp. 2584–2598, December 2016, doi: 10.1785/0120150361

Data-Driven Seismic-Hazard Models Prepared for a Seismic Risk Assessment in the Dead Sea Region

by Michael Haas, Amotz Agnon, Dino Bindi, Stefano Parolai, and Massimiliano Pittore

Abstract We derive a probabilistic seismic-hazard model for the Dead Sea region to allow for seismic risk estimation, which will be part of a subsequent study. This hazard model relies as much as possible on data-driven approaches, utilizing a seismic catalog compiled for the region by integrating data from different sources. We derive seismicity models using two different smoothing approaches and estimate a hypocentral depth distribution from historical observations. We do not include paleoseismological evidence apart from the observed seismicity. Because ground-motion records are sparse in the region, we formulate the model in the European Macroseismic intensity scale from 1998. However, the collected macroseismic intensity data are still too few to derive a local intensity prediction equation (IPE). Thus, we choose among existing equations derived for different regions and combine them in a logic tree. Here, motivated by Scherbaum *et al.* (2010), we propose a two-step approach to select the IPEs for the logic tree. First, we cluster a set of 10 candidate IPEs to identify groups of models that can be considered similar with respect to the distribution of the predicted values for a selection of the explanatory variables (i.e., magnitude and distance), using a *k*-mean approach (Steinhaus, 1956). Then, we apply different ranking techniques (Scherbaum *et al.*, 2009; Kale and Akkar, 2013) to identify within each cluster the most suitable model to be included in the logic tree. The resulting hazard models are consistent with existing probabilistic seismic-hazard models for the region. We estimate a moderate-to-high hazard of intensity grade VII–VIII with 10% probability of exceedance within 50 years in close vicinity to the Dead Sea transform fault, the dominant seismogenic structure in this region.

Introduction

The Dead Sea region is located in one of the most active tectonic regimes in the Middle East and thus greatly endangered by earthquakes. The largest tectonic feature in the region is the Dead Sea transform fault, running from the East Anatolian fault zone along the Jordan Valley, through the Dead Sea until the southern tip of the Sinai (see Fig. 1). The fault is the primary seismogenic structure of the plate boundary between the Sinai subplate and the Arabian plate (Salamon *et al.*, 1996). Because of the low slip rates of the two plates (4–6 mm/yr; Masson *et al.*, 2015), strong earthquakes (i.e., $M_w > 7$) are fortunately rare, but not impossible (one approximately every 250 years). The last earthquake causing severe damage for large parts of the region was the 1927 Jericho event with a local magnitude M_L 6.2 (Avni *et al.*, 2002) that only the elderly in today's population remember. Recently, the 1995 Nuweiba earthquake with a moment magnitude of M_w 7.2 that occurred in the Gulf of Aqaba reminded the population of the earthquake threat, although it caused limited damage due to its remote location (Hofstetter, 2003).

To understand the impact of future earthquakes of similar magnitude occurring closer to densely populated areas, a careful assessment of seismic risk is required. The three main risk components usually considered are (a) the hazard (i.e., the estimated probability of significant ground shaking caused by earthquakes), (b) the exposure (i.e., the population, buildings, and infrastructure that are at risk), and (c) the exposure's vulnerability to ground shaking (McGuire, 2004). This study sets out to establish the first component (i.e., the hazard) for the subsequent probabilistic seismic risk assessment in the region. To exemplify the resulting estimates in the region, we select cities that are of regional importance but are also small enough to allow a thorough assessment (population $< 150{,}000$) and are close to the Dead Sea transform fault. The selected cities are Eilat and Tiberias (Israel), Kerak and Madaba (Jordan), and Nablus and Ramallah (Westbank Palestine). There already exist several hazard models covering the region of interest (e.g., those by Jaradat *et al.*, 2008; Jimenez *et al.*, 2008; Grünthal *et al.*, 2009; Levi *et al.*, 2010; and Erdik *et al.*, 2012). Unfortunately, all of these models are only partly published

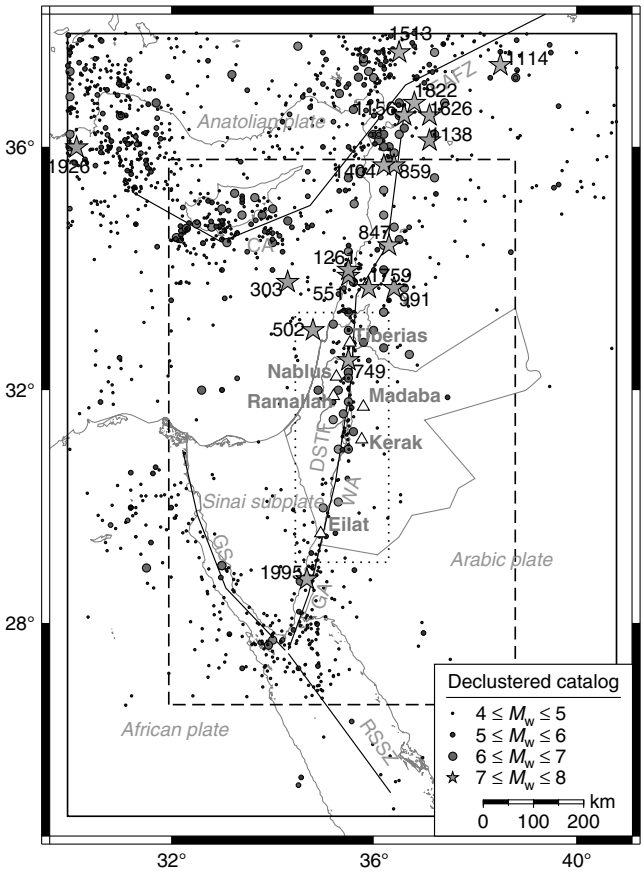

Figure 1. Selected sites for the hazard assessment (triangles), events ($M_w \geq 4$) contained in the catalog declustered with the Uhrhammer (1986) window and harmonized to M_w (circles, stars indicate strong events annotated with their year of occurrence) and the three different regions: catalog region (solid rectangle), source region (dashed rectangle), and hazard assessment region (dotted rectangle). The main features of the region's tectonics (black solid lines, modified from Salamon *et al.*, 1996) are also shown: RSSZ, Red Sea spreading zone; GS, Gulf of Suez; GA, Gulf of Aqaba; WA, Wadi Araba; DSTF, Dead Sea transform fault; CA, Cyprian arc; EAFZ, East Anatolian fault zone.

and hence not fully reproducible. We, therefore, decided to derive a new probabilistic seismic-hazard model to serve as input for a fully reproducible seismic risk assessment. For the derivation of this hazard model in the form of a probabilistic seismic-hazard assessment (PSHA, Cornell, 1968; McGuire, 1976), we rely on simple data-driven methods to guide the modeling decisions and implement the model in the free and open-source seismic hazard and risk platform OpenQuake, developed by the Global Earthquake Model (GEM) Foundation (Pagani *et al.*, 2014).

Methodology

A PSHA (Cornell, 1968; McGuire, 1976) is a method to estimate the hazard of ground shaking caused by earthquakes. To estimate the probabilities of ground-shaking levels, the historical seismicity, usually in the form of a catalog, is exploited to determine past and likely future sources of earthquakes, by modeling earthquake occurrence as a Poisson process. The magnitudes and average rates are usually determined via the Gutenberg–Richter law (Gutenberg and Richter, 1944) bounded by a minimum and maximum magnitude. The attenuation of the ground motion generated by the earthquakes at these sources is then approximated with empirical ground-motion prediction equations.

We opted not to use an area source model in the hazard assessment, because the delineation of these zones, intended to separate tectonic active regions into areas of homogeneous seismicity, involves many considerations and long scientific discussions among experts (Woo, 1996). Instead, we used a smoothed seismicity approach developing two different seismicity models using the schemes by Frankel (1995) and Woo (1996). Both methods make direct use of the historical seismic catalog and do not include paleoseismological evidence apart from this observed seismicity. This makes their application relatively simple, but can leave the resulting models vulnerable to lacking data. If not handled carefully, the applied smoothing may also yield an overly smeared hazard estimate.

Because our main focus is on the above-mentioned cities, we defined a target zone for the hazard assessment (see Fig. 1) as the rectangular region enclosing the cities and a 0.5° great-circle distance buffer zone around them. For an event of moment magnitude M_w 8, which is larger than any observed event in the study's region (M_w 7.5), using an intensity attenuation relation (Bindi *et al.*, 2011), we expect the macroseismic intensity to drop below an intensity VI (slightly damaging) on average within an epicentral distance of around 185 km. Thus, we define a seismic source-model region (Fig. 1) as the rectangular region around the cities with a 3° great-circle distance buffer. Considering seismicity within this source-model region ensures that at each point of the hazard assessment zone, potential events within at least 230 km distance are considered. Applying the smoothing kernels of the two smoothed seismicity methods on the boundaries of this source region makes it necessary to define a catalog region that is larger than the source region. For this calculation, we included two more degrees of great-circle distance (Fig. 1).

We estimate ground-motion levels using macroseismic intensity with intensity prediction equations (IPEs) instead of other available instrumental intensity measures such as, for example, peak ground acceleration (PGA) or spectral acceleration for two main reasons: (1) strong-motion data in the region are sparse (e.g., RESORCE database: 26 records for 8 earthquakes in Egypt, Israel, Lebanon, and Syria; Akkar *et al.*, 2014) in comparison with macroseismic intensity observations (675 observations for 82 events were collected for this study), and (2) the hazard model is to be integrated into a macroseismic-intensity-based risk assessment, in which the structural vulnerability will be estimated following the scheme of Giovinazzi and Lagomarsino (2004), which extends the empirical method proposed in the European Macroseismic scale from 1998 (EMS-98; Grünthal *et al.*, 1998). We refrain from using empirical relations (e.g., Worden *et al.*, 2012) to convert instrumental intensity measures, for example, PGA to macroseismic intensity since this would add another unnecessary

Table 1
Composition and Sources of the Catalog Declustered with the Uhrhammer Window

ID*	Source†	Events	Period	M_w Range	Missing z‡
1	Agnon (2014)	3	363–659	6.0–6.8	3
2	Marco *et al.* (2003)	1	749–749	7.3–7.3	1
3	Avni *et al.* (2002)	1	1927–1927	6.3–6.3	0
4	Sbeinati *et al.* (2005)	24	37–1822	6.1–7.5	1
5	Ambraseys (2006)	10	551–1872	6.0–7.2	5
6	Ambraseys and Adams (1993)	33	1894–1986	4.5–6.0	12
7	Grünthal and Wahlström (2012a)	732	1002–2006	4.0–7.5	145
8	GII	696	1905–2014	4.0–6.1	0
9	NCEDC b	476	1963–2014	4.0–6.1	0
10	ISC-GEM	2	1905–1914	5.6–7.0	0
11	IRIS	1268	1965–2014	4.0–6.1	2
12	ISC	2	1979–1984	5.6–7.0	0
13	KOERI	95	1903–2014	4.0–7.1	1
14	NCEDC a	9	1955–1994	4.0–5.7	0
15	Giardini *et al.* (2013)	20	1003–1997	4.1–6.8	19
16	GSHAP	10	23–1940	5.5–6.7	7
Total		3382	23–2014	4.0–7.5	196

*The ID represents the hierarchy (i.e., in case of duplicate events), which catalog was preferred over another, respecting the defined thresholds (see the Historical Seismicity section).

†GII, Earthquake in Israel bulletin; GSHAP, Seismic Catalog of Turkey and Neighbouring Countries of the Global Seismic Hazard Assessment Programme; IRIS, Incorporated Research Institutions for Seismology; FDSNWS-Event database; ISC, The Bulletin of the International Seismological Centre; ISC-GEM, ISC-GEM Global Instrumental Earthquake Catalogue v.1.05; KOERI, National Earthquake Monitoring Center EQ Catalog; NCEDC, Northern California Earthquake Data Center, Advanced National Seismic System (ANSS) Comprehensive Catalog accessed from two different query builders (a) and (b) (for details on all these data sources, see Data and Resources).

‡Number of events without depth estimates.

layer of uncertainty. We are aware that the assignment of macroseismic intensity, especially for older sources, leaves room for interpretation, and uncertainties in the macroseismic intensity estimates can thus become quite large, but in light of the previous considerations, we still regard them to be the better choice in this specific case. For calculation and visualization purposes, we treat macroseismic intensity values as decimal numbers throughout this study. These are not to be misinterpreted as actual values of macroseismic intensity, which are conventionally represented by categorized ordered variables (ordinals); for example, 5.9 and 6.3 are both intensity VI.

Historical Seismicity

To derive the seismicity models for this study, we compiled a catalog of historical earthquakes for the regions between 24.55° and 37.80° N and between 29.95° and 40.80° E (see Fig. 1) by integrating data from different sources.

Table 1 shows the catalogs considered for this study. We include only events in which epicenter and magnitude are given in the catalogs. Although this is only the first step in creating a hazard model, objective hazard assessment is hindered because the practice of the considered instrumental catalogs to publish earthquake location, magnitude, and focal mechanism estimates without uncertainties does not allow for a quantitative comparison of the different catalogs' quality. Thus, following the hierarchy given in Table 1 and using subjective time and distance thresholds (Table 2), we exclude duplicate entries originating from different catalogs. In general, we prefer complete hypocenter entries over incomplete ones. We assume that the coherence between the catalogs increases as the date of the events' occurrence approaches the present time, and thus we decrease the thresholds for time and location, distinguishing the period before 1000 C.E., the period until 1900, the early instrumental period since 1900, and the instrumental period since 1960. The hierarchy among the catalogs (ID in Table 1) is chosen based on the following assumptions: we assign the highest ranks to publications focusing on single or only a few historical events (ID 1–6), followed by one of the longest (1000 until 2006 C.E.), most reliable and complete available catalogs for the region, the European Mediterranean Earthquake Catalogue (EMEC; ID 7; Grünthal and Wahlström, 2012a; Grünthal and Wahlström, 2012b), followed by instrumental catalogs in which the highest rank is given to the local catalog of the Geophysical Institute of Israel (ID 8), followed by other global sources (ID 9–11), complemented with both purely instrumental catalogs (ID 12, 13), the Seismic Hazard Harmonization in Europe (SHARE) project catalog (SHEEC; Stucchi *et al.*, 2013; Grünthal *et al.*, 2013), as well as the Global Seismic Hazard Assessment Program (GSHAP) Turkey catalog (ID 14, 15). Interesting to note here is that some query builders, for example, NCEDC a and NCEDC b (Northern California Earthquake Data Center), which should query the same database, yield slightly different query results (for details on the data sources, see Data and Resources).

We considered characteristics of events that occurred B.C.E. too uncertain to contribute to this study's catalog.

Table 2
Time and Distance Thresholds, That If Not Exceeded Identify Duplicate Events in the Catalog

Period	Time	Distance (°)	Argument
Before 1000 C.E.	1 day	0.5	Many events only date available
1000–1899 C.E.	12 hours	0.4	Most events approximate time available
1900–1959	1 hour	0.3	Well documented
Since 1960	2 min	0.2	Instrumental catalogs

Table 3
Magnitude Conversion Relations Applied to the Original Magnitude Types in the Catalog

Magnitude	Conversion	SDR (M_w)*
M_s	Scordilis (2006)	0.17($M_s \leq 6.1$); 0.2($M_s \geq 6.2$)
M_L	Akkar *et al.* (2010)	0.2
M_b	Johnston (1996)	0.26
M_D/M_c	Çağnan and Kalafat (2012)	0.3

*Standard deviation of the residuals (SDR) determined by authors of the respective relation.

We include only a single magnitude type per event to create the catalog entry, in which the preference is in the following order: moment magnitude (M_w), surface magnitude (M_s), local magnitude (M_L), body-wave magnitude (M_b), and (coda-) duration magnitude (M_D, M_c). If the magnitude type of an event was specified as unknown we excluded it, and when depths were given with a value of zero we considered them to be artificial phenomena and removed them after manual revision.

We harmonized the resulting catalog to moment magnitude M_w using different conversion schemes. The different symbols for M_w, usually referring to the method of derivation, that is, M (unspecified derivation), M_{wb} (derived from body waves), M_{wc} (from coda waves), M_{wr} (regional moment magnitude), and M_{ww} (w-phase moment magnitude), were considered equivalent and despite their different underlying computation, considered to be equally scaled and therefore not converted. For the remaining encountered magnitude types, body (M_b), surface (M_s), local (M_L), and duration magnitudes (M_D, M_c), we used the conversions that Çağnan and Kalafat (2012) identified as being well suited for the eastern Mediterranean by conducting an analysis of variance for different relationships applied to data from the region (see Table 3). The resulting catalog, including 14,510 events above M_w 3, can be freely downloaded (Haas *et al.*, 2016) and will be updated within a versioning system in case novel research requires doing so.

Earthquake occurrence was modeled as a Poisson process, which implies the events' mutual independence. Because this is not the case for earthquake clusters, one has to remove foreshock and aftershock from the earthquake catalog. Thus, we applied the declustering algorithm proposed by Gardner and Knopoff (1974) to the catalog, in which we used once the space–time-window definition of Grünthal as reported by van Stiphout *et al.* (2012) and once the window as defined by Uhrhammer (1986). We assumed a foreshock time window half the size of the aftershock time window, which is approximately the ratio that one obtains using time windows defined in Burkhard and Grünthal (2009) up to magnitude 6.6 (0.44), then increasing to 1 at M_w 7.8. The number of remaining events above M_w 4 is 1908 for the Grünthal window and 3381 for the Uhrhammer window. We refer to these as the Grünthal and Uhrhammer catalogs for the remainder of the study. This step of declustering also ensures that any duplicated events that might have slipped through the thresholds defined for their identification are removed by the selection of the event with the largest magnitude (note that in this case, the hierarchy of the catalogs is not considered). The locations of the resulting Uhrhammer earthquake catalog for the region, covering events from year 23 until 2014 C.E., with magnitude larger or equal M_w 4 can be seen in Figure 1.

Table 4
Year of Completeness Estimates for 0.5 M_w Bins

	Grünthal Window Declustering*		Uhrhammer Window Declustering*	
M_w Bin Center	YBG†	YS‡	YBG†	YS‡
4.25	1987	1986	1987	1987
4.75	1963	1965	1965	1967
5.25	1945	1941	1935	1941
5.75	1895	1911	1895	1900
6.25	1870	1862	1860	1863
6.75	1000	606	1000	749
7.25	330	552	330	577

*For both declustered versions of the catalog.
†Year of completeness using visual method by Burkhard and Grünthal (2009, referred to as YBG).
‡Year of completeness using the Stepp (1972) method, referred to as YS.

We estimated catalog completeness using a visual approach; that is, plotting the cumulative number of earthquakes in 0.5 M_w magnitude bins versus years and, as described in Burkhard and Grünthal (2009), identifiying the year of completeness (referred to as YBG) as the year in which the rate significantly changes. We compared the resulting years of completeness with estimates obtained from the Stepp (1972, referred to as YS) approach as defined in Makropoulos and Burton (1981), employing 0.5 magnitude bins and 10-year time intervals. Both approaches show a good agreement until M_w 6.5. The estimated completeness times for the declustered catalogs can be found in Table 4. Figure 2a shows the completeness magnitudes resulting from the visual analysis of a subset of the Uhrhammer catalog since 1750.

Smoothed-Seismicity Source Models

We decided to use a smoothed seismicity approach for earthquake rate estimation and implemented, among the avail-

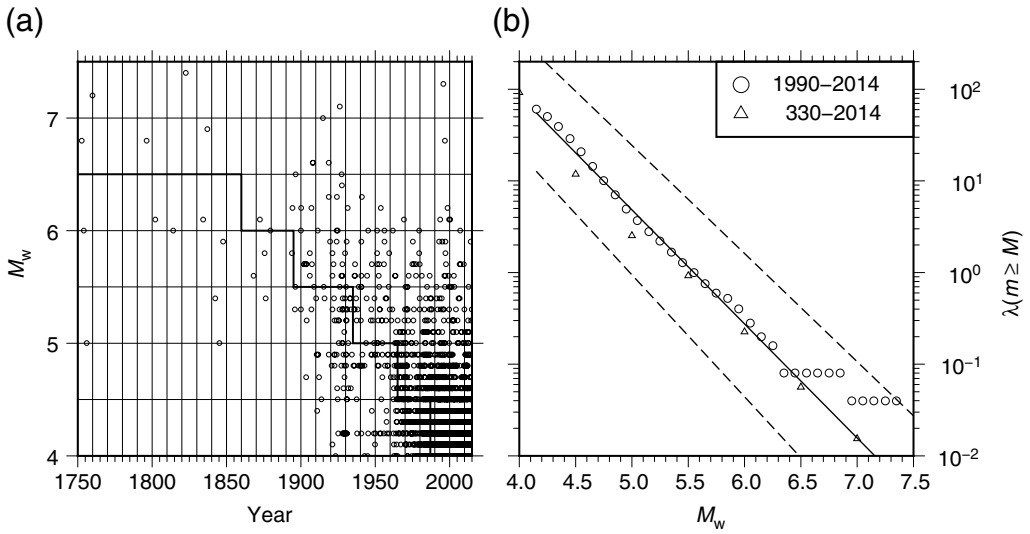

Figure 2. (a) Events from the Uhrhammer catalog since 1750 and the estimated years of completeness (see YBG values in Table 4); that is, the catalog is considered to be complete above the line. (b) Recurrence models from a Monte Carlo simulation with 10,000 iterations accounting for magnitude uncertainties: average annual rate (including foreshock and aftershock) since 1990 (circles), mean estimated Gutenberg–Richter model for the whole catalog region (solid line) using the Uhrhammer catalog, 95% confidence interval of the Gutenberg–Richter model (dashed lines). The maximum-likelihood Gutenberg–Richter parameters estimated with Aki–Utsu (Aki, 1965; Utsu, 1965) are $a = 6.92 \pm 0.17$ and $b = 1.25 \pm 0.04$ for the Uhrhammer catalog. For comparison, the observed annual rate estimated from the complete parts of the Uhrhammer catalog in 0.5 M_w bins are plotted alongside (triangles).

able methods, the ones proposed by Frankel (1995) and Woo (1996). First, we derived a seismic source model based on the gridded seismicity approach following Frankel (1995). Because this approach requires one to model the magnitude–frequency distribution of earthquakes according to the Gutenberg–Richter law (Gutenberg and Richter, 1944), we decided to employ a double-truncated version with a minimum magnitude of M_w 4, a single regional b-value, and a single regional maximum magnitude. Assuming time invariance, we used the most complete part of both declustered catalogs (i.e., events since 1990) to estimate a regional b-value. Excluding events below M_w 4, we estimated the magnitude of completeness (M_c) for this part of the catalog using the median-based analysis of the segment slope method by Amorese (2007) and applied an Aki–Utsu (Aki, 1965; Utsu, 1965) maximum-likelihood estimator to the events above this magnitude. To account for uncertainties in the magnitude, we considered a rounding error of 0.1, assuming a uniform distribution, whereas for uncertainties associated with the applied magnitude conversions (see Table 3), we assumed a normal distribution. Running Monte Carlo simulations with 10,000 iterations on these distributions, we obtained a b-value distribution with a mean of 1.12 (standard deviation $\sigma = 0.04$), a mean a-value of 6.14 ($\sigma = 0.18$) for an average magnitude of completeness $M_c = 4.2$ for the Grünthal catalog, a b-value distribution with mean 1.25 ($\sigma = 0.04$), and a mean a-value of 6.92 ($\sigma = 0.17$) for an average $M_c = 4.1$ using the Uhrhammer catalog. Figure 2b shows the estimated Gutenberg–Richter law for the Uhrhammer catalog in 0.1 M_w steps and its 95% confidence interval in comparison with the mean of the observed rates (which vary with the magnitude sampling) from the catalog since 1990. In addition, the observed rate estimated from the complete part of the Uhrhammer catalog since 330 is shown. Acknowledging concerns about assigning a maximum magnitude (Holschneider *et al.*, 2011; Zöller *et al.*, 2013, 2014), we estimated a maximum magnitude using the Bayesian estimator by Kijko (2004) of M_w 8. Inserting this estimate into the nontruncated version of the Gutenberg–Richter relation we obtained, we can estimate an average return period of an event larger than M_w 8 as 660 years (Grünthal catalog; Uhrhammer catalog 1200) for the whole region. Because such a magnitude event has probably not been observed in the region for the last 2000 years, we consider it safe to use it as the maximum magnitude. In the following, the a-values estimated along with the b-values are not considered.

Instead, we estimate the spatial distribution of the seismic activity rate by applying the Frankel (1995) method as follows: the catalog region is split into a grid of 0.1° by 0.1° and, using the declustered catalogs spanning from the year 23 until 2014, we quantify for each grid cell the observed seismicity. The count for each cell is then adjusted for catalog incompleteness (YBG values in Table 4) by employing our b-value estimates in the Herrmann (1977) formula and adding expected seismicity below the minimum magnitude of the catalog. Accounting for errors in earthquake location and allowing for a potential future variation in location, we smoothed the observed seismicity for each of the cells over neighboring cells using a Gaussian kernel with three different bandwidths of 15, 20, and 25 km.

As a second smoothing method, we applied the Woo (1996) approach to the catalog. The Woo (1996) method differs from the Frankel (1995) method in two main ways: (1) the

rate of earthquake occurrence is estimated for each event separately using the effective return period and (2) the Vere-Jones (1992) power law is used for the rate smoothing. By considering only the complete part of the catalog, the effective return period for each event can be approximated with the time between the year of completeness of its magnitude (see the Historical Seismicity section) and the end of the catalog. In the power law by Vere-Jones (1992), instead of using a fixed width Gaussian kernel, we employed, as outlined in Woo (1996), a magnitude (M)-dependent smoothing kernel $h(M)$ of the form:

$$h(M) = H \times \exp(k \times M). \quad (1)$$

We estimated the parameters H and k for the region using a Monte Carlo simulation on the magnitude uncertainties similar to the Frankel (1995) approach. In addition to the conversion uncertainties, we estimated an average magnitude uncertainty of 0.5 M_w for pre-1900 events by analyzing the duplicates identified during the catalog creation with at least four estimates. We determined for each of 1000 iterations the average between-event distances via least squares for the complete part (Table 4, YBG) of both declustered catalogs. Using 0.5 M_w bins, we obtained a mean $H = 1.98 \pm 0.67$ and mean $k = 0.52 \pm 0.07$ for the Grünthal catalog and $H = 0.44 \pm 0.14$ and $k = 0.73 \pm 0.06$ for the Uhrhammer catalog. Because the Woo (1996) approach makes use of the fractal pattern of earthquake occurrence through the Vere-Jones (1992) kernel, the fractal dimension has to be estimated, which can be approximated by the correlation exponent, which we estimated alongside the H and k values as $\nu = 1.701 \pm 0.014$ (Grünthal catalog) and $\nu = 1.640 \pm 0.008$ (Uhrhammer catalog) following Grassberger and Procaccia (1983) and Hirata (1989).

Assuming normal distribution for location errors in longitude and latitude as well as for magnitude uncertainties, we considered the same distance values used for identifying duplicates in the catalog as the standard deviation for epicentral location (see the Historical Seismicity section). The Woo (1996) method, in addition, considers the magnitude uncertainties we described for the kernel estimation for each event separately during the rate estimation. We estimated the rate using a kernel with the mean H and k, as well as kernels with plus and minus one standard deviation of these parameters.

Figure 3 shows the resulting rates for M_w 4 and 6 events for both methods using the Uhrhammer catalog and mean parameters: (a) Frankel (1995): $b = 1.25$, 20 km smoothing and (b) Woo (1996): $H = 0.44, k = 0.73, \nu = 1.64$. Although the two methods yield quite similar rates for the smaller magnitudes, the differences between the models increase for larger magnitudes. This is due to the use of a regional b-value in the Frankel (1995) method. In places where we observe many, mainly small events in the catalog (M_w 4–5, see Fig. 1), for example, along the Wadi Araba and the Gulf of Aqaba (with the exception of M_w 7.2 in 1995), the Frankel (1995) method yields a high a-value and in combination with the regionally

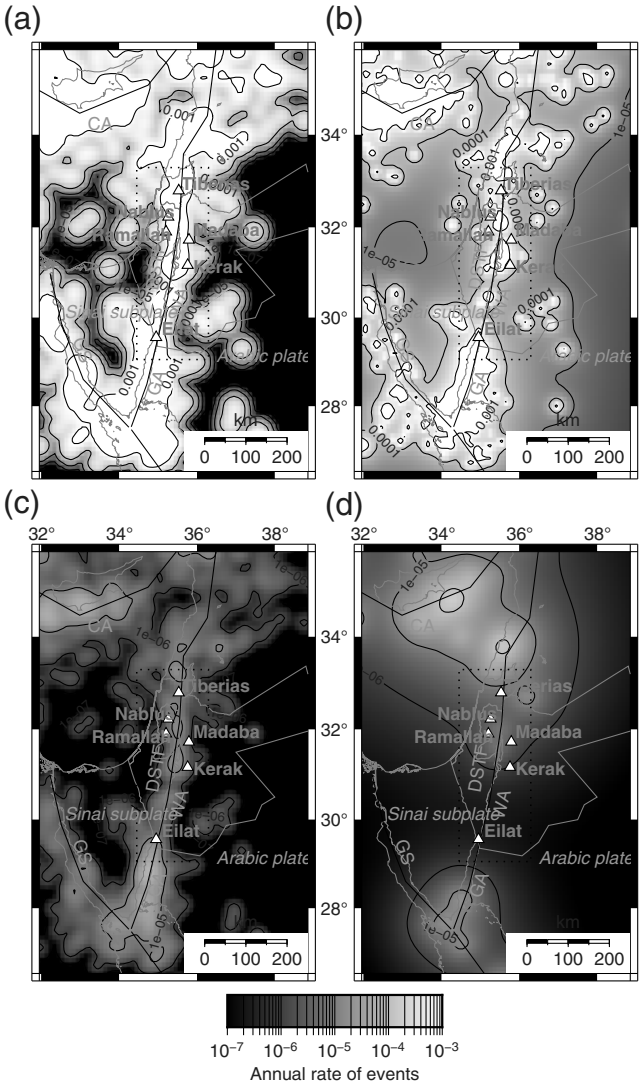

Figure 3. Rates estimated from the Uhrhammer catalog on a 0.1° by 0.1° grid for (a,b) M_w 4 and (c,d) M_w 6 using in (a) and (c) the Frankel (1995) ($\sigma = 20$ km, truncated at 3σ, $b = 1.25$, $M_{wmin} = 4$ and $\Delta M_w = 0.2$) and using in (b) and (d) the Woo (1996) approach ($H = 0.44$, $k = 0.73$, $\nu = 1.64$, $M_{wmin} = 4$, and $\Delta M_w = 0.2$).

estimated b-value (not capturing this behavior), the model expects also larger earthquakes in these regions. In case of the Woo (1996) approach, these larger events are not modeled because they are not present in the catalog. This leads to the observed differences between both models for larger magnitude events in these regions. The lack of large observed events in these regions might well be an artifact of the particular locations, because they are less populated and thus less monitored than other areas in the study region.

On the other hand, most of the larger events ($M_w > 6.5$) tend to be located in the northern half of the model region, which yields higher rates for these larger events using Woo (1996), then for the Frankel (1995) method whose regional b-value does not capture this clustering.

We developed the rates considering only longitude and latitude; thus, to account for hypocentral distance in the

Table 5
Depth Distribution Using Events Since 1900

Longitude*	Latitude*	0–5 (km)	5–15 (km)	15–30 (km)	30–50 (km)
31.95	26.55	0.18	0.54	0.19	0.09
31.95	30.55	0.10	0.52	0.27	0.11
31.95	34.55	0.04	0.35	0.35	0.26
31.95	38.55	0.11	0.39	0.20	0.30
35.95	26.55	0.23	0.65	0.10	0.02
35.95	30.55	0.18	0.67	0.11	0.04
35.95	34.55	0.23	0.53	0.12	0.12
35.95	38.55	0.15	0.51	0.14	0.20
39.95	26.55	0.22	0.65	0.09	0.04
39.95	30.55	0.19	0.59	0.14	0.08
39.95	34.55	0.16	0.58	0.15	0.11
39.95	38.55	0.14	0.59	0.11	0.16

Determined from the 100 events closest to the points (longitude, latitude) given in the table.
*Cell centers of a 4° by 4° grid over the catalog region.

ground-motion estimation, we estimated a hypocentral depth distribution from the seismic catalog. For this purpose, we considered only events occurring since 1900. As expected, for a mainly transform fault regime with a crustal thickness of around 32–37 km (Hofstetter *et al.*, 2000), almost 80% of these events occurred at a depth shallower than 50 km. Most (75%) of the deeper events, with a focal depth greater than 50 km, are close to the subduction regime of the Cyprian arc on the western side of the East Anatolian fault zone. Thus, for reasons of simplicity and assuming that the region of interest is mostly endangered by shallow earthquakes, we restricted the model to account only for the shallow crustal events with a depth of up to 50 km. To estimate an earthquake depth distribution from these events, the catalog was divided into 12 4° by 4° cells to allow for stable results. For each of the cells, a discretized depth distribution, shown in Table 5, was then estimated from the historical depth distribution. Each point in our source models therefore inherits the depth distribution of the closest point of this grid.

Macroseismic Intensity Prediction

As outlined in the Methodology section, we used macroseismic intensity as the ground-motion intensity measure. We collected macroseismic intensity estimates and their locations for historical events within a slightly larger region than our catalog region (i.e., in modern day Israel, Jordan, Lebanon, Palestine, Syria, and southeast Turkey). We collected the data from (1) historic intensity estimates in EMS-92 (Sbeinati *et al.*, 2005), (2) estimates from Guidoboni *et al.* (1994) and Guidoboni and Comastri (2005), (3) data from the 1927 Jericho event (Zohar and Marco, 2012), and (4) the isoseismal map of the 1995 Aqaba earthquake (Al-Tarazi, 2000). Because the exact location of the observations is not published in the latter, we used the location of settlements with more than 5000 inhabitants within 10 km distance from each isoseismal as observed intensity locations. We considered the collected intensity values, assigned in EMS-92, EMS-98, or modified Mercalli intensity, as equivalent (Musson *et al.*, 2010). The values given in Sbeinati *et al.* (2005) for regions, rather than exact names of settlements (e.g., Syria, Iraq, Egypt, etc.), were not considered. In case of duplicated event information from the different sources, we preferred the source with more information (i.e., intensity estimates for more locations). In total, we collected 675 intensity observations from 82 events for the region. The complete version of the data set can be found in Haas *et al.* (2016).

For further analysis, we restricted ourselves to C.E. event observations with a maximal epicentral distance of 200 km and a minimum intensity of 5. Furthermore, using, for example, the Bindi *et al.* (2011) IPE, we estimated the probability of exceeding intensity 7.5 at an epicentral distance of 150 km as less than 1%, and thus we excluded all observations with intensity values greater than 7.5 at distances larger than 150 km. In case the intensity observation is given with minimal and maximal values, we used their mean. Applying these reductions left us with 442 observations for 64 events since 23 C.E., with M_w between 4.8 and 7.9, in which 158 observations were for the two events in 1927 and 1995 C.E.

An attempt to derive a regional IPE from these data employing a mixed-effect regression model (Abrahamson and Youngs, 1992) yielded no robust regression result and was therefore not used here.

To account for epistemic uncertainty in the prediction of the intensity measure selected for hazard assessments, it is common practice to combine alternative models derived for other regions through a logic-tree approach. The logic tree combines the models in a probabilistic way, that is, with which probability each model should contribute to the hazard estimate. The concept of a logic tree is to capture the epistemic uncertainty in a model, and thus the selected IPEs should best describe the ground motion observed in the region, while at the same time avoiding redundancy. Which models are chosen for implementation is often based on the visual analysis of data fits or on the application of ranking methods (e.g., as proposed by Scherbaum *et al.*, 2009, and Kale and Akkar, 2013). The problem with this approach is that simply choosing the best ranking or best-fitting models might lead to the selection of very similar and therefore dependent models (Scherbaum *et al.*, 2010). This is in contradiction of the fundamental idea behind the logic tree, in which the models implemented in the different branches should be mutually exclusive and collectively exhaustive (Bommer and Scherbaum, 2008). Here, motivated by Scherbaum *et al.* (2010), we proposed a simple two-stage approach for selecting empirical attenuation models that are not too similar but still perform well for our region. In the first step, we clustered available attenuation relations by similarity using a *k*-means cluster method (Steinhaus, 1956) on IPE estimates over a discrete parameter space. Then, in the second step, we applied ranking methods (Scherbaum *et al.*, 2009; Kale and Akkar, 2013) to our collected intensity data to select a single representative model from each of the resulting clusters. We

Table 6
Considered Intensity Prediction Equations (IPEs), their Performance for Three Measures, Similarity Cluster, and Weights

ID	IPE	rmsR	LLH	EDR	Cluster*	SS†	W‡
2	Bakun (2006)	1.32 (5)§	−4.28 (6)	1.96 (7)	a	791	0
5	Dowrick and Rhoades (2005)	1.11 (2)	−4.90 (9)	1.44 (3)	a	791	0
6	Sørensen *et al.* (2009)	1.00 (1)	−2.20 (1)	1.45 (4)	a	791	0.25
9	Sørensen *et al.* (2010)	1.51 (8)	−3.03 (3)	2.31 (8)	a	791	0
10	Gasperini *et al.* (2010)	1.22 (3)	−2.87 (2)	1.37 (2)	b	230	0.25
8	Pasolini *et al.* (2008)	1.23 (4)	−3.08 (4)	1.50 (5)	b	230	0
4	Chandler and Lam (2002)	1.38 (6)	−5.85 (10)	1.77 (6)	c	0	0.25
1	Allen *et al.* (2012)	1.76 (10)	−4.13 (5)	3.33 (10)	d	53	0
3	Bindi *et al.* (2011)	1.60 (9)	−4.49 (8)	2.93 (9)	d	53	0.25
7	Le Goff *et al.* (2014)	1.45 (7)	−4.46 (7)	1.36 (1)	e	0	0

rmsR, root mean square residuals; LLH, log-likelihood method (Scherbaum *et al.*, 2009); EDR, Euclidean distance ranking (Kale and Akkar, 2013).
*Similarity cluster IPE belongs to.
†Within cluster sum of squares (SS).
‡Assigned weight in the logic-tree framework of the hazard model.
§Rank of IPE in braces for each measure.

applied the two-step approach to 10 IPEs (Table 6) to define the logic-tree branches for the Dead Sea region.

In the first step, we identified similarities among the considered IPEs and then investigated their performance against the collected intensity data. To identify their similarity, we discretized the model parameter space into 0.1 magnitude steps from M_w 5 to 7.5 and 5-km epicentral distance steps from 5 to 200 km. Based on this discretization, we estimated for each magnitude–distance pair and IPE the predicted mean macroseismic intensity value and its standard deviation (Scherbaum *et al.*, 2010); because intensity estimates are normally distributed random variables, these fully describe the distributions. Applying a k-means clustering algorithm to the 10 resulting vectors with 1040 values each, we attempted to find clusters with similar IPEs. For the two boundary cases, in which either all IPEs are in one cluster (i.e., number of clusters $k = 1$) or all but two are in a separate cluster (i.e., $k = 9$), the sum of squares (SS) within the cluster is 11,771 and 53 for the cases $k = 1$ and $k = 9$, respectively. Thus, by minimizing the within-class SS for all 10 clusters, we identify five clusters, a, b, c, d, and e (i.e., $k = 5$), in an iterative procedure with a maximum SS of 791 (cluster a) within any one of the clusters, as shown in Table 6. Using a 2D visualization technique for multidimensional data as also described in Scherbaum *et al.* (2010), Figure 4a shows Sammon's map (Sammon, 1969) of the IPEs' mean estimates on the discretized parameter space. The distance between the models corresponds to the Euclidean distance between the predictor vectors for the means. Figure 4a thus allows us to visually identify the grouping resulting from the k-means cluster algorithm.

In the second step, we tested the 10 IPEs against the collected intensity observations. Because for most of the events focal mechanisms or rupture estimates are not available, we used only epicentral and hypocentral distances. If a depth estimate was missing, we fixed the depth to 10 km, corresponding to the historical median depth in the catalog. We evaluated the IPEs' performance using three different measures: (1) the root mean square residuals (rmsR), (2) the log-likelihood method (LLH; Scherbaum *et al.*, 2009), and (3) the Euclidean distance ranking (EDR; Kale and Akkar, 2013).

Although the LLH method is based on computing the log likelihood of the observations given the respective IPE as probability density function, the EDR method is based on the Euclidean distance between predicted and observed intensity while considering a systematic first-order model bias. In all cases, a value closer to zero stands for better performance considering the given data. As one can see from Table 6, considering each of the measures separately would result in very different rankings (e.g., Dowrick and Rhoades, 2005, rmsR = 2, LLH = 9, EDR = 3; or Sørensen *et al.*, 2010, rmsR = 8, LLH = 3, EDR = 8). However, as we rely on the similarity between the IPEs as identified by the clustering, we chose only one IPE for each of the identified clusters. Figure 4b–f shows for each cluster the estimates of each IPE for an M_w 7.25 event at 10 km depth, plotted against the observed historical intensities for the largest events in the region between M_w 7 and 7.5. For the first cluster a, we selected Sørensen *et al.* (2009) because, with exception of the EDR, in which it ranks second, this IPE was ranked highest within the cluster. For the second cluster b, we chose Gasperini *et al.* (2010) because it consistently ranked higher than Pasolini *et al.* (2008). In cluster d, Bindi *et al.* (2011) was chosen because only LLH would rank Allen *et al.* (2012) higher. From the single IPE clusters (c and d), we implement only Chandler and Lam (2002) because, although Le Goff *et al.* (2014) fits well for smaller events, it is applicable only to $M_w \leq 6.2$ and, as Figure 4f shows, it strongly overestimates the intensity for large M_w.

Logic Tree for the Hazard Model

As stated above, we used a logic-tree approach to consider epistemic uncertainty in our hazard models. We employed a

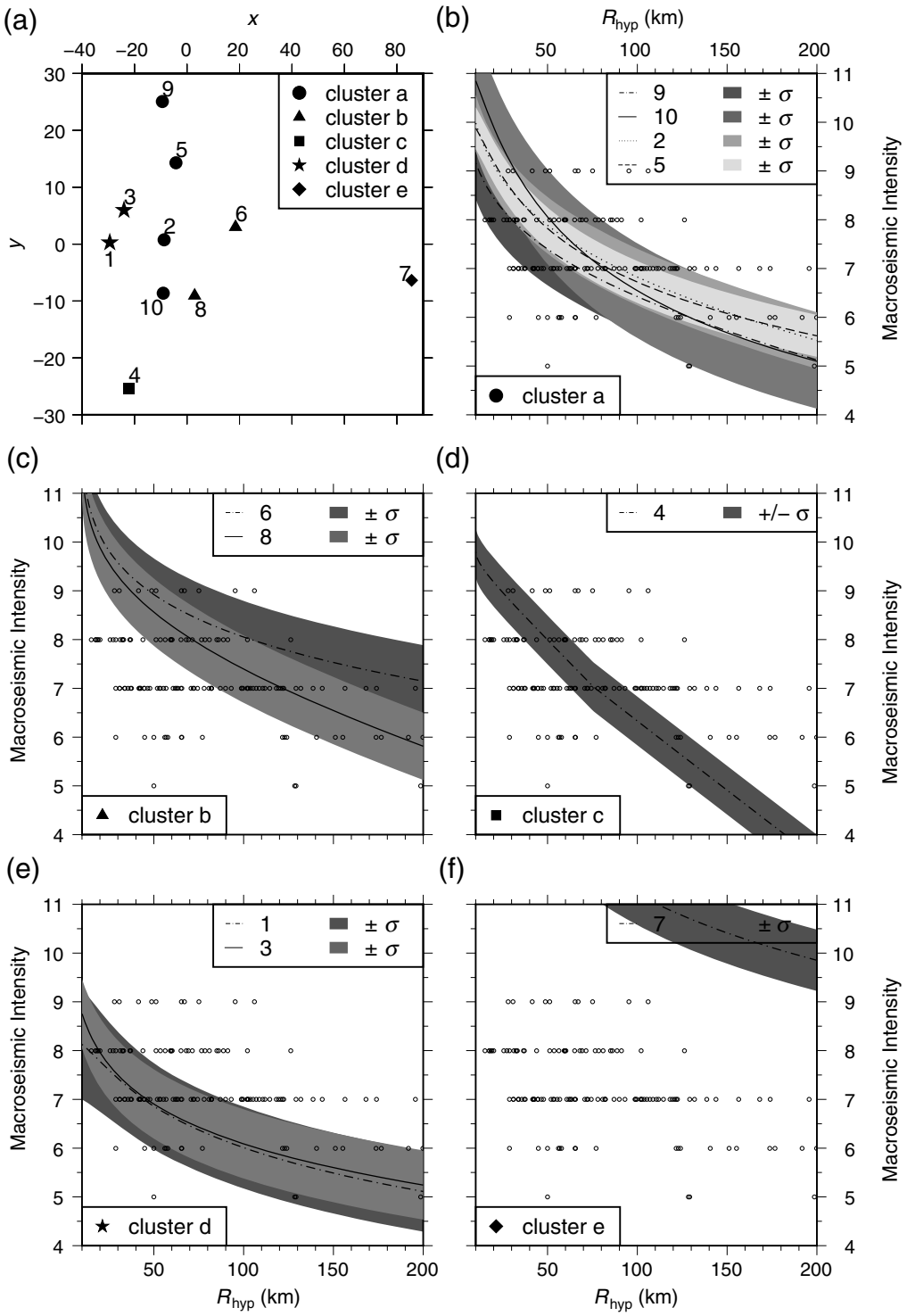

Figure 4. (a) Sammon's map (Sammon, 1969) of the 10 considered intensity prediction equations (IPEs); the symbols indicate the cluster that each IPE belongs to, according to a *k*-means clustering (Steinhaus, 1956) of the mean and standard deviations of their estimates over discrete parameter space. (b)–(f) Estimated mean (curves) and $\pm 1\sigma$ (shaded) intensity attenuation resulting from each IPE in each cluster for an M_w 7.25 event at 10 km depth against historical distance intensity pairs for events with M_w 7.0–7.5. IPE IDs are (see also Table 6) 1, Allen *et al.* (2012); 2, Bakun (2006); 3, Bindi *et al.* (2011); 4, Chandler and Lam (2002); 5, Dowrick and Rhoades (2005); 6, Gasperini *et al.* (2010); 7, Le Goff *et al.* (2014); 8, Pasolini *et al.* (2008); 9, Sørensen *et al.* (2009); 10, Sørensen *et al.* (2010).

logic tree that consists of two layers: one layer for the epistemic uncertainty in the source model and one layer for the uncertainty in the intensity attenuation relation. For the Frankel model, the source-model logic tree considers the two different declustered catalogs (equal probability), a variation of the *b*-value using the mean (40% probability) and ± 1 standard deviation

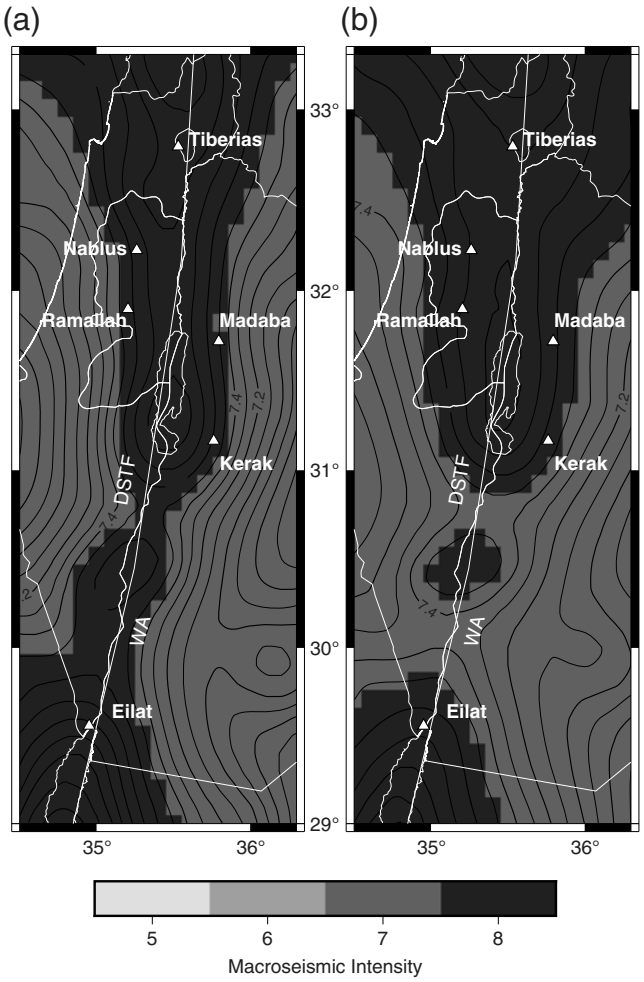

Figure 5. 10% probability of exceedance within any 50 years using (a) the Frankel (1995) based model and (b) the Woo (1996) based model.

(30% probability each), a variation of the estimated M_{max} by 0.25 ($M_{max} = 7.75$ with probability $p = 30\%$, $M_{max} = 8.0$ with $p = 40\%$, and $M_{max} = 8.25$ with $p = 30\%$), and varying the smoothing bandwidth with 15, 20, and 25 km (equal probability). For the Woo (1996) method, we considered both declustered catalogs (equal probability) and allowed the coefficients of the magnitude-dependent kernel to vary, taking the mean values (40%) and ± 1 standard deviation (30% each). We did not consider the uncertainty of the fractal dimension because the small variation estimated for each catalog has only a marginal impact on the kernel.

The second branching level of the logic tree is intended to capture the epistemic uncertainty in the attenuation relation. Although Scherbaum *et al.* (2009) suggest a way to weight the different models, they also warn that this is only mathematically valid in the theoretical case of infinite observations. This brings the model's derivation to a point where subjectivity is hard to avoid. Because a fully probabilistic approach for the weighting is not possible, we assign equal weights to all of the IPEs we implemented as representative for their clusters.

Resulting Hazard Estimates

We implemented both models as point-source models in the OpenQuake software (Pagani *et al.*, 2014) and estimated the hazard for the selected target hazard region (see Fig. 1).

From Figure 5a, we can see that according to the Frankel (1995) based model in any 50-year time frame, an intensity of VIII (i.e., up to 8.5) is expected to be exceeded with 10% probability in the region. The highest values of hazard are expected along the Dead Sea transform fault, with slightly lower values along the Wadi Araba. The estimates based on the Woo (1996) model (Fig. 5b) are very similar, even indistinguishable in large parts of the model region, considering the ordinal nature of the macroseismic intensity scale. Nevertheless, we like to use a continuous scale to discuss the small differences that result from the application of the different approaches. We observed differences as already expected from the rate comparison discussed in the Smoothed Seismicity Source Models section (Fig. 3). The hazard in the Frankel model (Fig. 5a) is higher along the Wadi Araba and the Gulf of Aqaba due to the use of a regional *b*-value, which, in combination with a high seismicity, tends to create stronger events, even though they were not observed in the past. Furthermore, we found a pronounced spread of the hazard for the Woo (1996) method in the northern part of the model, which is due to the greater number of observed large events in the north (see Figs. 1 and 3). Overall, the Woo (1996) method yields a slightly higher (~0.2 intensity degrees) hazard over large parts of the model, with the exception of the Wadi Araba and the Gulf of Aqaba.

If we compare the annual mean hazard curves of the selected locations shown in Figure 6, we observe that for Frankel (1995; Fig. 6a) and Woo (1996; Fig. 6b), the differences between the locations do not exceed half an intensity value. The differences do not increase significantly when going from higher to lower rates. In the Frankel (1995) model (Fig. 6a), Eilat and Tiberias have the highest hazard among the six locations and Madaba and Ramallah the lowest, whereas Nablus and Kerak exhibit values ranging between those of the other locations. According to the Woo model (Fig. 6b), Eilat, as already expected from the results shown in Figure 5, is assigned a lower hazard than in the Frankel (1995) model, with increasing difference when going to longer return periods (10%: 0.1, 2%: 0.3). The highest hazard is consistently estimated with the Frankel (1995) model for Tiberias. Also, the estimation of Karak as having the lowest hazard is consistent, whereas Madaba, on the lower side in the Frankel (1995) approach, is modeled with a medium hazard. In Figure 6a, the dark shaded area depicts the uncertainty of the two extremes, Madaba and Tiberias, as the 5% and 95% quantiles for the hazard curves, showing a range of up to 2 intensity degrees at rates corresponding to a 2475-year average return period. The logic tree of the Woo (1996) based model is not large enough to allow for the estimation of the quantiles and is thus not indicated in Figure 6b.

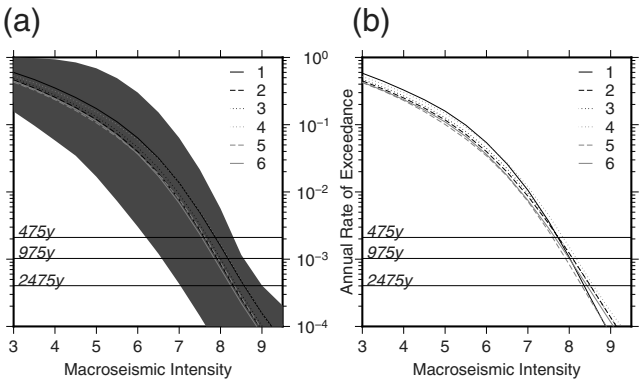

Figure 6. Resulting mean annual hazard curves for Eilat (1), Ramallah (2), Nablus (3), Tiberias (4), Karak (5), and Madaba (6) for (a) the Frankel (1995) model and (b) the Woo (1996) model. The dark shaded part in (a) is bounded by the 5% quantile of the lowest hazard curve and the 95% quantile of the largest hazard (shaded). The horizontal lines represent mean annual rates equivalent to 2% (2475-year return period), 5% (975 years), and 10% (475 years) probability of exceedance over a 50-year time period.

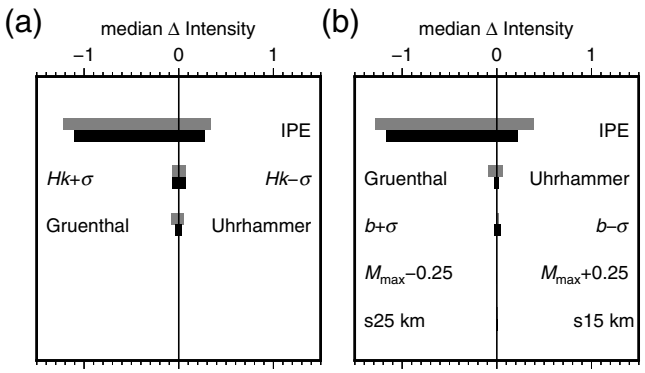

Figure 7. Sensitivity analysis of the different model parameters for (a) the Woo (1996) model and (b) the Frankel (1995) based model. Bars are for mean hazard with 10% (gray) and 5% (black) probability of exceedance within 50 years.

Discussion and Comparison to Other Models

We performed a sensitivity analysis of the model parameters for both models. Figure 7a shows the median difference for the six locations in terms of intensity for the Woo (1996) model. The strongest deviation results from the IPE applied, followed by the size of the smoothing kernel and finally by the choice of the declustering window. For IPE choice and declustering, the difference is larger for shorter return periods (gray bars, 475 years; black bars, 975 years). The differences for the Frankel (1995) model are shown in Figure 7b. Although the influence of the IPE remains similar, the size of the smoothing window has almost no influence (order of ~0.01 intensity). We observed a stronger sensitivity to changes in the declustering method with respect to the Woo (1996) model. Obviously, the effect of the b-value variation is more pronounced for the longer return periods due to the logarithmic shape of the Gutenberg–Richter law. The influence of M_{max} is negligible as for the smoothing (~0.02 intensity degrees).

We compare the results of our model with the hazard model proposed for the region by Jaradat *et al.* (2008) and with the outcomes of the GSHAP project (Giardini *et al.*, 1999).

The Jaradat *et al.* (2008) model is almost fully reproducible with the exception of the depth distribution. We adopt this model's area source zones with a, b, and maximum magnitudes as described therein, but because the depth distribution was unclear we took the depth distribution for each source zone from our estimated distribution. Implementing this model in OpenQuake (Pagani *et al.*, 2014) with our IPE logic tree, we observed estimated intensity differences in the resulting hazard estimates at a 475-year return period with respect to the Frankel (1995) based model as shown in Figure 8a. The largest differences are in the Gulf of Aqaba, where we found up to one intensity higher estimates in the area source model. In contrast, for the northern part of the model region, the area source model shows hazard between 0.6 and 0.2 intensity grades lower than our Frankel (1995) based model.

Figure 8b shows the difference between the results of the GSHAP project for the region (Giardini *et al.*, 1999), where we converted the published peak ground acceleration values to macroseismic intensity using an empirical relationship from Worden *et al.* (2012) and the Frankel (1995) based model. For large parts of the study area, our model yields higher hazard estimates, with a difference ranging between 0.2, close to the fault, to up to 1.4 intensity values. The most remarkable difference can be observed in the south of Jordan (southeast of Ma'an), where the Frankel (1995) based model exceeds the GSHAP estimate by almost 2 intensity grades. This area is an active mining region (Mahmoud Al-Quaryouti, personal comm., 2015, from the Jordan Seismological Observatory), but because events below M_w 4 are not considered in the estimate, we assume that any event possibly related to the mining activity is already excluded from the model. Overall, the differences between the two models increase from north to south and west to east.

Figure 9a,b shows the mean hazard curves for Eilat and Madaba resulting from the Frankel (1995) model, the Woo (1996) model, and the Jaradat *et al.* (2008) based model. The curves for Eilat show the behavior as expected from the hazard map comparison: Jaradat *et al.* (2008) yields the highest, followed by Frankel (1995) and Woo (1996) in which the differences increase for longer return periods. For Madaba, the situation is different, because Woo (1996) yields the highest and Jaradat *et al.* (2008) the lowest hazard. Although the difference between the Jaradat *et al.* (2008) and the Frankel (1995) model decreases with smaller annual rates, the difference between the latter and the Woo (1996) model increases. At an average return period of 475 years, the Woo (1996) estimate is closer to the Frankel (1995) based estimates, whereas at 2475 years, the Woo (1996) estimate is closer to Jaradat *et al.* (2008).

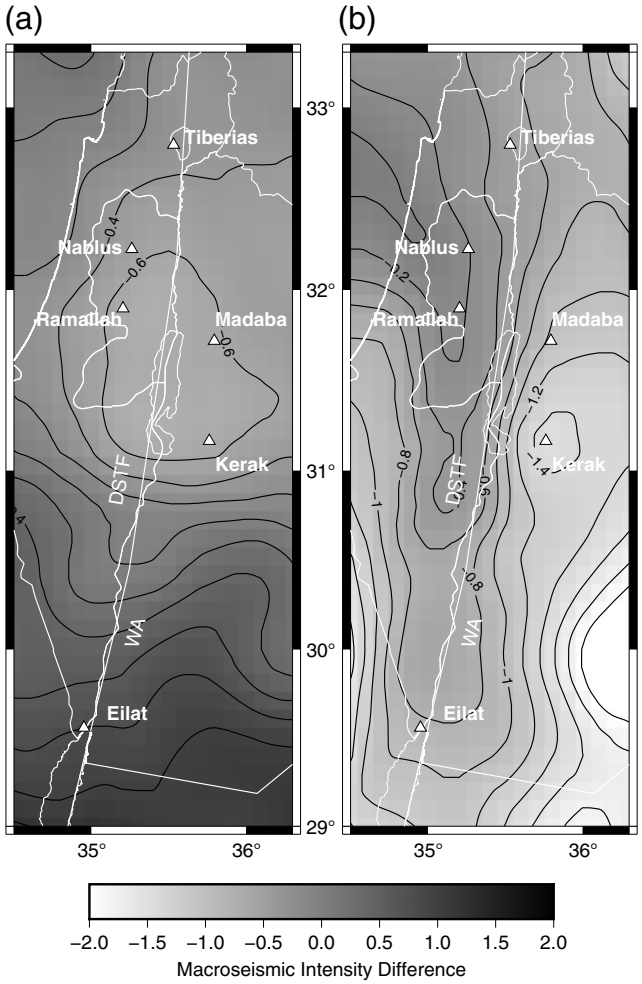

Figure 8. Differences in the intensity estimates with 10% probability of exceedance within 50 years between (a) a model using an area source seismicity model by Jaradat *et al.* (2008), in which depth was estimated from our depth model and our logic tree for the IPEs was employed, and the Frankel (1995) based model, and (b) between the results of the Global Seismic Hazard Assessment Program (GSHAP) project (Giardini *et al.*, 1999), converted from peak ground acceleration to macroseismic intensity using Worden *et al.* (2012), and the Frankel (1995) model.

Conclusion

Following a data-driven approach, we implemented two smoothed-seismicity-based hazard models using both the Frankel (1995) and Woo (1996) methods while considering uncertainties in location and magnitude in the historical seismicity records, but not considering paleoseismological evidence apart from the observed seismicity. Although deriving purely data-driven hazard models seems theoretically feasible, the study shows that many obstacles remain, especially for regions with few instrumental data. In particular, the use of catalogs that do not include uncertainties in their estimates leads to subjective choices in their priority in case of duplicates. Moreover, the sparse available ground-motion data in the region forcibly lead to subjective choices with respect to

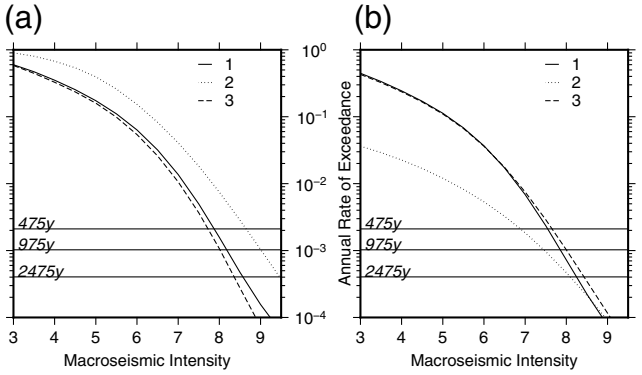

Figure 9. Mean hazard curves estimated from the different models for the cities of (a) Eilat and (b) Madaba. The models are 1, using the Frankel (1995) based model; 2, estimates based on the Jaradat *et al.* (2008) model; and 3, model derived following the Woo (1996) method.

intensity attenuation relations. We tried to minimize this subjectivity by implementing a two-stage approach combining the concept of identifying similarities between empirical attenuation models (Scherbaum *et al.*, 2010) and performance ranking methods (Scherbaum *et al.*, 2009; Kale and Akkar, 2013). We proposed employing a *k*-means cluster algorithm (Steinhaus, 1956) on the discrete parameter model to identify similarity. The downside of this approach is that the number of classes has to be set in advance. We identified the number of classes in an iterative way, which might be more challenging if the set of considered attenuation relations were larger. The weighting of the models in the logic tree still remains a challenge since we treated the clusters as independent and equally probable, the latter is an especially crude simplification.

We found, as expected, that magnitude-dependent smoothing methods, such as the Woo (1996) approach, may treat regions dominated by a high seismicity with mainly small magnitudes more consistently than a Frankel (1995) based model with a regional *b*-value. A further optimization might be achieved by applying smoothing windows that adapt their size to the near seismicity instead of using a fixed bandwidth (e.g., Stock and Smith, 2002), as shown recently in Moschetti *et al.* (2014) and Ullah *et al.* (2015). Summarizing the findings of the Frankel (1995) and Woo (1996) based hazard assessment, we found a moderate-to-high hazard of intensity grade VII–VIII for 10% probability of exceedance within 50 years close to the Dead Sea transform fault, and of intensity VII for the remaining part of the region. Comparing the hazard estimates of our models to the results of other models for the region, we found that the application of simple, data-driven methods such as the Frankel (1995) or Woo (1996) approach allows for the derivation of reasonable and consistent probabilistic hazard estimates in the discussed region. We concluded that these hazard models can be employed within the framework of seismic risk assessment. Future studies shall thus focus on the derivation of exposure and vulnerability models for the selected locations and shall

provide an estimate for the seismic risk within a consistent end-to-end framework based on this study's hazard model.

Data and Resources

Seismic event data, besides those published in the literature and listed in the references, were collected from the following sources: the Earthquake in Israel bulletin, available from the Geophysical Institute of Israel at http://seis.gii.co.il/en/earthquake/searchEQS.php (last accessed January 2015); the Seismic Catalog of Turkey and Neighbouring Countries of the Global Seismic Hazard Assessment Program available from the ETH Zürich at http://www.seismo.ethz.ch/static/gshap/turkey/seisgshap.prn (last accessed January 2015); the FDSNWS-Event database available from Incorporated Research Institutions for Seismology (IRIS) at http://service.iris.edu/fdsnws/event/1/ (last accessed January 2015); the Bulletin of the International Seismological Centre (ISC) available from ISC at http://www.isc.ac.uk/iscbulletin/search/catalogue/ (last accessed January 2015); the ISC-GEM Global Instrumental Earthquake Catalogue v.1.05 available from the International Seismological Centre, Thatcham, United Kingdom, at http://www.isc.ac.uk/iscgem/request_catalogue.php (last accessed January 2015); the National Earthquake Monitoring Center EQ Catalog available from Bogazici Üniversitesi Kandilli Observatory and Earthquake Research Institute (KOERI) at http://www.koeri.boun.edu.tr/sismo/zeqdb/indexeng.asp (last accessed January 2015); and the Advanced National Seismic System (ANSS) Comprehensive Catalog available from the Northern California Earthquake Data Center (NCEDC), UC Berkeley Seismological Laboratory at http://earthquake.usgs.gov/earthquakes/search/ and http://quake.geo.berkeley.edu/anss/catalog-search.html (last accessed January 2015).

Acknowledgments

This research was conducted within the Dead Sea Research Venue (DESERVE) virtual institute funded by the Helmholtz Association of German Research Centers. Models were implemented and calculated using Global Earthquake Model's (GEM) OpenQuake software tool (Pagani *et al.*, 2014) and some of the routines defined in the Hazard Modeller's Toolkit (Weatherill, 2014). The regression analysis was performed using lme4 (Bates *et al.*, 2015). For plotting, the Generic Mapping Tool (GMT; Wessel and Smith, 1991) was used. Special thanks to Kevin Fleming and Shahid Ullah for their most valuable suggestions and comments. Many thanks also to an anonymous reviewer and Laurentiu Danciu, whose suggestions greatly improved this study.

References

Abrahamson, N. A., and R. R. Youngs (1992). A stable algorithm for regression analyses using the random effects model, *Bull. Seismol. Soc. Am.* **82,** no. 1, 505–510.

Agnon, A. (2014). Pre-instrumental earthquakes along the Dead Sea rift, in *Dead Sea Transform Fault System: Reviews*, Z. Garfunkel, Z. Ben-Avraham, and E. Kagan (Editors), Vol. 6, Springer, Dordrecht, The Netherlands, 207–261.

Aki, K. (1965). Maximum likelihood estimate of b in the formula $\log N = a - bM$ and its confidence limits, *Bull. Earthq. Res. Inst.* **43,** 237–239.

Akkar, S., Z. Çağnan, E. Yenier, Ö. Erdoğan, M. A. Sandıkkaya, and P. Gülkan (2010). The recently compiled Turkish strong motion database: Preliminary investigation for seismological parameters, *J. Seismol.* **14,** no. 3, 457–479, doi: 10.1007/s10950-009-9176-9.

Akkar, S., M. A. Sandıkkaya, M. Şenyurt, A. Azari Sisi, B. Ö. Ay, P. Traversa, J. Douglas, F. Cotton, L. Luzi, B. Hernandez, *et al.* (2014). Reference database for seismic ground-motion in Europe (RESORCE), *Bull. Earthq. Eng.* **12,** no. 1, 311–339, doi: 10.1007/s10518-013-9506-8.

Allen, T. I., D. J. Wald, and C. B. Worden (2012). Intensity attenuation for active crustal regions, *J. Seismol.* **16,** no. 3, 409–433.

Al-Tarazi, E. (2000). The major Gulf of the Aqaba earthquake, 22 November 1995—Maximum intensity distribution, *Nat. Hazards* **22,** no. 1, 17–27.

Ambraseys, N. N. (2006). Comparison of frequency of occurrence of earthquakes with slip rates from long-term seismicity data: The cases of Gulf of Corinth, Sea of Marmara and Dead Sea fault zone, *Geophys. J. Int.* **165,** no. 2, 516–526, doi: 10.1111/j.1365-246X.2006.02858.x.

Ambraseys, N. N., and R. D. Adams (1993). Seismicity of the Cyprus region, *Terra Nova* **5,** no. 1, 85–94.

Amorese, D. (2007). Applying a change-point detection method on frequency–magnitude distributions, *Bull. Seismol. Soc. Am.* **97,** no. 5, 1742–1749, doi: 10.1785/0120060181.

Avni, R., D. Bowman, A. Shapira, and A. Nur (2002). Erroneous interpretation of historical documents related to the epicenter of the 1927 Jericho earthquake in the Holy Land, *J. Seismol.* **6,** no. 4, 469–476.

Bakun, W. H. (2006). MMI attenuation and historical earthquakes in the basin and range province of western North America, *Bull. Seismol. Soc. Am.* **96,** no. 6, 2206–2220, doi: 10.1785/0120060045.

Bates, D., M. Maechler, B. Bolker, and S. Walker (2015). Fitting linear mixed-effects models using lme4, *J. Stat. Softw.* **67,** no. 1, 1–48, doi: 10.18637/jss.v067.i01.

Bindi, D., S. Parolai, A. Oth, K. Abdrakhmatov, A. Muraliev, and J. Zschau (2011). Intensity prediction equations for Central Asia: Intensity attenuation model for Central Asia, *Geophys. J. Int.* **187,** no. 1, 327–337, doi: 10.1111/j.1365-246X.2011.05142.x.

Bommer, J. J., and F. Scherbaum (2008). The use and misuse of logic-trees in probabilistic seismic hazard analysis, *Earthq. Spectra* **24,** no. 4, 997–1009.

Burkhard, M., and G. Grünthal (2009). Seismic source zone characterization for the seismic hazard assessment project PEGASOS by the Expert Group 2 (EG1b), *Swiss J. Geosci.* **102,** no. 1, 149–188.

Çağnan, Z., and D. Kalafat (2012). A new catalogue of eastern Mediterranean earthquakes, 2150 BC-2011, *Proc. of 15th World Conference on Earthquake Engineering*, Lisbon, Portugal.

Chandler, A. M., and N. T. Lam (2002). Intensity attenuation relationship for the South China region and comparison with the component attenuation model, *J. Asian Earth Sci.* **20,** no. 7, 775–790, doi: 10.1016/S1367-9120(01)00054-2.

Cornell, C. A. (1968). Engineering seismic risk analysis, *Bull. Seismol. Soc. Am.* **58,** no. 5, 1583–1606.

Dowrick, D. J., and D. A. Rhoades (2005). Revised models for attenuation of modified Mercalli intensity in New Zealand earthquakes, *Bull. New Zeal. Soc. Earthq. Eng.* **38,** no. 4, 185–214.

Erdik, M., K. Şeşetyan, M. B. Demircioğlu, C. Tüzün, D. Giardini, L. Gülen, D. S. Akkar, and M. Zare (2012). Assessment of seismic hazard in the Middle East and Caucasus: EMME (Earthquake Model of Middle East) project, *Proc. of 15th World Conference on Earthquake Engineering*, Lisbon, Portugal.

Frankel, A. (1995). Mapping seismic hazard in the central and eastern United States, *Seismol. Res. Lett.* **66,** no. 4, 8–21.

Gardner, J. K., and L. Knopoff (1974). Is the sequence of earthquakes in southern California, with aftershocks removed, Poissonian, *Bull. Seismol. Soc. Am.* **64,** no. 5, 1363–1367.

Gasperini, P., G. Vannucci, D. Tripone, and E. Boschi (2010). The location and sizing of historical earthquakes using the attenuation of macroseismic intensity with distance, *Bull. Seismol. Soc. Am.* **100,** no. 5A, 2035–2066, doi: 10.1785/0120090330.

Giardini, D., T. Cameelbeeck, G. Grünthal, R. Basili, B. Glavatovic, G. Valensise, H. Crowley, A. Campos-Costa, C. Meletti, J. Woessner, *et al.*

(2013). Seismic Hazard Harmonization in Europe (SHARE): Online data resource, doi: 10.12686/SED-00000001-SHARE.

Giardini, D., G. Grünthal, K. M. Shedlock, and P. Zhang (1999). The GSHAP global seismic hazard map, *Ann. Geophys.* **42,** no. 6, doi: 10.4401/ag-3784.

Giovinazzi, S., and S. Lagomarsino (2004). A macroseismic method for the vulnerability assessment of buildings, *13th W. Conf. Earthq. Eng.*, Vancouver, British Colombia, Canada, 1–6.

Grassberger, P., and I. Procaccia (1983). Measuring the strangeness of strange attractors, *Physica D.* **9,** no. 1/2, 189–208.

Grünthal, G., and R. Wahlström (2012a). The European-Mediterranean Earthquake Catalogue (EMEC) for the last millennium, *J. Seismol.* **16,** no. 2, doi: 10.1007/s10950-012-9302-y.

Grünthal, G., and R. Wahlström (2012b). EMEC Earthquake catalogue, GFZ Data Services, doi: 10.5880/GFZ.EMEC.001.

Grünthal, G., A. Hakimhashemi, H. Schelle, C. Bosse, and R. Wahlström (2009). The long-term temporal behaviour of the seismicity of the Dead Sea fault zone and its implication for time-dependent seismic hazard assessments, *Sci. Tech. Rept. No. 09/09*, Deutsches GeoForschungsZentrum GFZ, Potsdam, Germany.

Grünthal, G., R. Musson, J. Schwarz, and M. Stucchi (1998). European macroseismic scale 1998 (EMS-98), in *Cahiers du Centre Européen de Géodynamique et de Séismologique*, Vol. 15, Centre Européen de Géodynamique et de Séismologie, Luxembourg.

Grünthal, G., R. Wahlström, and D. Stromeyer (2013), The SHARE European Earthquake Catalogue (SHEEC) for the time period 1900–2006 and its comparison to EMEC, *J. Seismol.* **17,** no. 4, 1339–1344, doi: 10.1007/s10950-013-9379-y.

Guidoboni, E., and A. Comastri (2005). *Catalogue of Earthquakes and Tsunamis in the Mediterranean Area from the 11th to the 15th Century*, Istituto Nazionale di Geofisica e Vulcanologia, Rome, Italy.

Guidoboni, E., A. Comastri, G. Traina, and Istituto nazionale di geofisica (Italy) (Editors) (1994). *Catalogue of Ancient Earthquakes in the Mediterranean Area up to the 10th Century*, Istituto Nazionale di Geofisica e Vulcanologia, Rome, Italy.

Gutenberg, B., and C. F. Richter (1944). Frequency of earthquakes in California, *Bull. Seismol. Soc. Am.* **34,** no. 4, 185–188.

Haas, M., A. Agnon, D. Bindi, S. Parolai, and M. Pittore (2016). DESERVE earthquake catalogue and macroseismic intensity dataset, GFZ Data Services, doi: 10.5880/GFZ.7.1.2016.001.

Herrmann, R. B. (1977). Recurrence relations, *Seismol. Res. Lett.* **48,** nos. 1/2, 47–49, doi: 10.1785/gssrl.48.1-2.47.

Hirata, T. (1989). A correlation between the b value and the fractal dimension of earthquakes, *J. Geophys. Res.* **94,** no. B6, 7507–7514.

Hofstetter, A. (2003). Seismic observations of the 22/11/1995 Gulf of Aqaba earthquake sequence, *Tectonophysics* **369,** no. 1, 21–36.

Hofstetter, A., C. Dorbath, M. Rybakov, and V. Goldshmidt (2000). Crustal and upper mantle structure across the Dead Sea rift and Israel from teleseismic P-wave tomography and gravity data, *Tectonophysics* **327,** nos. 1/2, 37–59, doi: 10.1016/S0040-1951(00)00161-X.

Holschneider, M., G. Zöller, and S. Hainzl (2011). Estimation of the maximum possible magnitude in the framework of a doubly truncated Gutenberg–Richter model, *Bull. Seismol. Soc. Am.* **101,** no. 4, 1649–1659, doi: 10.1785/0120100289.

Jaradat, R. A., O. K. Nusier, M. M. Awawdeh, M. Y. Al-Qaryouti, Y. M. Fahjan, and A. M. Al-Rawabdeh (2008). Deaggregation of probabilistic ground motions for selected Jordanian cities, *Jord. J. Civil Eng.* **2,** 172–196.

Jimenez, M., H. Al-Nimry, A. Khasawneh, T. Al-Hadid, and K. Kahhaleh (2008). Seismic hazard assessment for Jordan and neighbouring areas, *Bull. Geof. Teor. Appl.* **49,** 17–36.

Johnston, A. C. (1996). Seismic moment assessment of earthquakes in stable continental regions-I. Instrumental seismicity, *Geophys. J. Int.* **124,** no. 2, 381–414, doi: 10.1111/j.1365-246X.1996.tb07028.x.

Kale, O., and S. Akkar (2013). A new procedure for selecting and ranking ground-motion prediction equations (GMPEs): The Euclidean distance-based ranking (EDR) method, *Bull. Seismol. Soc. Am.* **103,** no. 2A, 1069–1084, doi: 10.1785/0120120134.

Kijko, A. (2004). Estimation of the maximum earthquake magnitude, m_{max}, *Pure Appl. Geophys.* **161,** no. 8, 1655–1681, doi: 10.1007/s00024-004-2531-4.

Le Goff, B., J. F. Borges, and M. Bezzeghoud (2014). Intensity-distance attenuation laws for the Portugal mainland using intensity data points, *Geophys. J. Int.* **199,** no. 2, 1278–1285, doi: 10.1093/gji/ggu317.

Levi, T., B. Tavron, O. Katz, R. Amit, D. Segal, Y. Hamiel, Y. Bar-Lavi, S. Romach, and A. Salamon (2010). Earthquake loss estimation in Israel using the new HAZUS-MH software: Preliminary implementation, *Report GSI/11/2010*, The Ministry of National Infrastructures—Geological Survey of Israel, Jerusalem, Israel.

Makropoulos, K. C., and P. W. Burton (1981). A catalogue of seismicity in Greece and adjacent areas, *Geophys. J. Int.* **65,** no. 3, 741–762.

Marco, S., M. Hartal, N. Hazan, L. Lev, and M. Stein (2003). Archaeology, history, and geology of the AD 749 earthquake, Dead Sea transform, *Geology* **31,** no. 8, 665–668.

Masson, F., Y. Hamiel, A. Agnon, Y. Klinger, and A. Deprez (2015). Variable behavior of the Dead Sea fault along the southern Arava segment from GPS measurements, *C. R. Geosc.* **347,** no. 4, 161–169, doi: 10.1016/j.crte.2014.11.001.

McGuire, R. K. (1976). FORTRAN computer program for seismic risk analysis, *U.S. Geol. Surv. Open-File Rept. No. 76-77*, United States Department of the Interior Geological Survey.

McGuire, R. K. (2004). *Seismic Hazard and Risk Analysis*, Earthquake Engineering Research Institute, Oakland, California.

Moschetti, M. P., C. S. Mueller, O. S Boyd, and M. D. Petersen (2014). Development of an adaptively smoothed seismicity model for Alaska and implications for seismic hazard, *Proc. of the 10th U.S. National Conference on Earthquake Engineering*, Earthquake Engineering Research Institute, Anchorage, Alaska.

Musson, R. M. W., G. Grünthal, and M. Stucchi (2010). The comparison of macroseismic intensity scales, *J. Seismol.* **14,** no. 2, 413–428, doi: 10.1007/s10950-009-9172-0.

Pagani, M., D. Monelli, G. Weatherill, L. Danciu, H. Crowley, V. Silva, and D. Vigano (2014). OpenQuake engine: An open hazard (and risk) software for the global earthquake model, *Seismol. Res. Lett.* **85,** no. 3, 692–702, doi: 10.1785/0220130087.

Pasolini, C., D. Albarello, P. Gasperini, V. D'Amico, and B. Lolli (2008). The attenuation of seismic intensity in Italy, Part II: Modeling and validation, *Bull. Seismol. Soc. Am.* **98,** no. 2, 692–708, doi: 10.1785/0120070021.

Salamon, A., A. Hofstetter, Z. Garfunkel, and H. Ron (1996). Seismicity of the eastern Mediterranean region: Perspective from the Sinai subplate, *Tectonophysics* **263,** no. 1, 293–305.

Sammon, J. W. (1969). A nonlinear mapping for data structure analysis, *IEEE Trans. Comp*, **C-18,** no. 5, 401–409.

Sbeinati, M. R., R. Darawcheh, and M. Mouty (2005). The historical earthquakes of Syria: An analysis of large and moderate earthquakes from 1365 BC to 1900 AD, *Ann. Geophys.* **48,** no. 3, 347–435.

Scherbaum, F., R. Delavaud, and C. Riggelsen (2009). Model selection in seismic hazard analysis: An information-theoretic perspective, *Bull. Seismol. Soc. Am.* **99,** no. 6, 3234–3247, doi: 10.1785/0120080347.

Scherbaum, F., N. M. Kuehn, M. Ohrnberger, and A. Koehler (2010). Exploring the proximity of ground-motion models using high-dimensional visualization techniques, *Earthq. Spectra* **26,** no. 4, 1117–1138, doi: 10.1193/1.3478697.

Scordilis, E. M. (2006). Empirical global relations converting M_s and m_b to moment magnitude, *J. Seismol.* **10,** no. 2, 225–236, doi: 10.1007/s10950-006-9012-4.

Sørensen, M., D. Stromeyer, and G. Grünthal (2009). Attenuation of macroseismic intensity: A new relation for the Marmara Sea region, northwest Turkey, *Bull. Seismol. Soc. Am.* **99,** no. 2A, 538–553.

Sørensen, M. B., D. Stromeyer, and G. Grünthal (2010). Intensity attenuation in the Campania region, Southern Italy, *J. Seismol.* **14,** no. 2, 209–223, doi: 10.1007/s10950-009-9162-2.

Steinhaus, H. (1956). Sur la division des corps matériels en parties, *Bull. Acad. Polon. Sci.* **4 (CL III),** no. 12, 801–804 (in French).

Stepp, J. C. (1972). Analysis of the completeness of the earthquake sample in the Puget Sound area and its effect on statistical estimates of earthquake hazard, *Proc. of the Intern. Conf. Microzon. Safer Constr.: Research and Application*, Seattle, Washington, Vol. 64, 1189–1207.

Stock, C., and E. G. Smith (2002). Adaptive kernel estimation and continuous probability representation of historical earthquake catalogs, *Bull. Seismol. Soc. Am.* **92,** no. 3, 904–912.

Stucchi, M., A. Rovida, A. A. Gomez Capera, P. Alexandre, T. Camelbeeck, M. B. Demircioglu, P. Gasperini, V. Kouskouna, R. M. W. Musson, M. Radulian, *et al.* (2013). The SHARE European Earthquake Catalogue (SHEEC) 1000-1899, *J. Seismol.* **17,** no. 2, 523–544, doi: 10.1007/s10950-012-9335-2.

Uhrhammer, R. A. (1986). Characteristics of northern and central California seismicity, *Earthq. Notes* **57,** no. 1, 21.

Ullah, S., D. Bindi, M. Pilz, L. Danciu, G. Weatherill, E. Zuccolo, and S. Parolai (2015). Probabilistic seismic hazard assessment for Central Asia, *Ann. Geophys.* **58,** no. 1, doi: 10.4401/ag-6687.

Utsu, T. (1965). A method for determining the value of b in a formula $\log n = a–bM$ showing the magnitude–frequency relation for earthquakes, *Geophys. Bull. Hokkaido University* **13,** 99–103.

van Stiphout, T., J. Zhuang, and D. Marsan (2012). Seismicity declustering, doi: 10.5078/corssa-52382934.

Vere-Jones, D. (1992). Statistical methods for the description and display of earthquake catalogues, in *Statistics in the Environmental and Earth Sciences*, A. T. Walden and P. Guttorp (Editors), Edward Arnold, London, 220–246.

Weatherill, G. A. (2014). *Hazard Modeller's Toolkit—User Guide*, Technical Report, Global Earthquake Model (GEM).

Wessel, P., and W. H. Smith (1991). Free software helps map and display data, *Eos Trans. AGU* **72,** no. 41, 441–448.

Woo, G. (1996). Kernel estimation methods for seismic hazard area source modeling, *Bull. Seismol. Soc. Am.* **86,** no. 2, 353–362.

Worden, C. B., M. C. Gerstenberger, D. A. Rhoades, and D. J. Wald (2012). Probabilistic relationships between ground-motion parameters and modified Mercalli intensity in California, *Bull. Seismol. Soc. Am.* **102,** no. 1, 204–221, doi: 10.1785/0120110156.

Zohar, M., and S. Marco (2012). Re-estimating the epicenter of the 1927 Jericho earthquake using spatial distribution of intensity data, *J. Appl. Geophys.* **82,** 19–29, doi: 10.1016/j.jappgeo.2012.03.004.

Zöller, G., M. Holschneider, and S. Hainzl (2013). The maximum earthquake magnitude in a time horizon: Theory and case studies, *Bull. Seismol. Soc. Am.* **103,** no. 2a, 860–875, doi: 10.1785/0120120013.

Zöller, G., M. Holschneider, S. Hainzl, and J. Zhuang (2014). The largest expected earthquake magnitudes in Japan: The statistical perspective, *Bull. Seismol. Soc. Am.* **104,** no. 2, 769–779, doi: 10.1785/0120130103.

GFZ German Research Centre for Geosciences
Telegrafenberg
Potsdam D-14473, Germany
mhaas@gfz-potsdam.de
(M.H., D.B., S.P., M.P.)

Institute of Earth Sciences
Hebrew University of Jerusalem
Jerusalem 91904, Israel
(A.A.)

Manuscript received 8 December 2015;
Published Online 15 November 2016